SLAC-PUB-6047
January 1993
(T/E)

THE DIRC COUNTER: A NEW TYPE OF PARTICLE IDENTIFICATION DEVICE FOR B FACTORIES*

BLAIR RATCLIFF

Stanford Linear Accelerator Center, Stanford University, Stanford, CA 94309 USA

ABSTRACT

A very thin, solid radiator, totally internally reflecting, imaging Cherenkov counter (DIRC) is described. This device is well matched to the hadronic charged particle identification requirements at an asymmetric e^+e^- B Factory.

1. INTRODUCTION

Particle identification at a B factory is difficult, and highly constrained by the machine environment and the need for good energy measurement of soft photons in the calorimeter which surrounds the particle identification device [1]. Because of the high beam crossing rate and the potential for large backgrounds, the particle identification detector must be robust and relatively fast. Good π/K separation is required over a wide momentum range between about 0.25 and 4 GeV/c. Most detectors measure dE/dx in the tracking chamber which allows good π/K separation up to about 600 MeV/c, but a specific identification device is required over most of the momentum region [2]. The amount of material in the device should be small (preferably less than 10% L_{RAD}) and should be distributed as close as possible to the calorimeter in order to avoid degradation in the resolution performance of the calorimeter, and the loss of low energy conversion electrons in the magnetic field. In addition, the cost of the high quality calorimeter scales roughly like the radius squared and there will be substantial cost savings if the particle identification device can be made thin.

Here, we describe a new type of imaging Cherenkov (the DIRC) that appears to be extremely well matched to the requirements for particle identification at the B factory. It is thin (with low radiation length), robust, very fast, and should have excellent performance over the complete phase space of the B factory. Although many configurations of a DIRC type device are possible, for definiteness, a particular straw-man model will be discussed which uses quartz radiator bars, read–out by conventional photomultiplier tubes in a proximity focused geometry. A brief discussion of some possible variations will follow within the space limitations here. More details can be found elsewhere [3].

2. THE DIRC IMAGING PRINCIPLE

The geometry of a single radiator of the DIRC is shown schematically in Fig. 1. Each radiator is a long, thin, flat "bar" with rectangular cross section [t_x, t_y]. There is a photodetection surface positioned some distance (ℓ) away from the end of the bar. A track with velocity β passing through the radiator with refractive

* Work supported by Department of Energy, contract DE–AC03–76SF00515.

Presented at the International Workshop on B Factories: Accelerators and Experiments, Tsukuba, Japan, November 17-20, 1992

index n_1 emits Cherenkov radiation in a cone around the particle trajectory with cone half angle θ_C given by the Cherenkov relation

$$\cos\theta_C = \frac{1}{n_1\beta} \quad . \qquad (1)$$

The angles, positions, and momentum of the track are provided by a tracking device located in front of the radiator. If the index of refraction of the radiating material (n_1) exceeds $\sqrt{2}$, and n_3 is approximately 1, some portion of the light will always be transported down the "bar" to the end for a particle close to $\beta = 1$,. Since the radiator cross section is rectangular, angles are maintained in reflections at the surfaces of the bar (up to the additional up-down/left-right ambiguity). Thus, in a perfect bar, the portion of the Cherenkov cone that lies inside the total internal reflection angle is transported undistorted down the bar to the end. When it reaches the end, the light either reflects or emerges into a standoff region with index n_2. It then travels some distance until it hits a two–dimensional detection surface, where it forms an image on the surface as shown in Fig. 2. The image is essentially a conic section of the cone–modified by refraction at the n_1, n_2 interface. It has been "doubled" by the up-down reflection ambiguity. In the case shown, the track enters the radiator in the y-z plane so that the left and right going images are symmetrical. Since the locus of the image depends on the polar and azimuthal Cherenkov angles (θ_C, ϕ_C), particle identification using Cherenkov angular information can proceed using essentially the same hypothesis testing techniques employed by imaging Cherenkov devices of the RICH/CRID type [4].

Two different image loci are shown in Fig. 2 corresponding to different extremes for the width t_x of the bar, as shown schematically in Fig. 1. In the extreme limit of the PLATE geometry, the bar is sufficiently wide that no reflections occur from the sides of the bar,

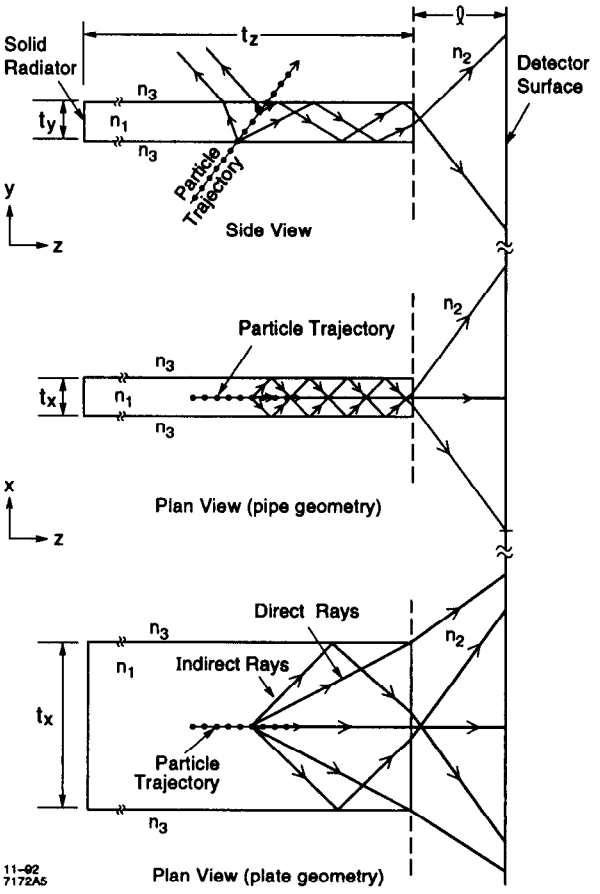

Figure 1. Schematic of a radiator bar of the DIRC counter for two different radiator widths (pipe and plate) described in the text; the particle trajectory is shown as a line connected by dots; representative trajectories of Cherenkov photons are shown by lines with arrows.

so there is no left-right imaging ambiguity. That is, the "indirect" rays shown in Fig. 1 do not emerge from the end. In the other limit, the PIPE geometry, the bar width t_x is much smaller than the photon measurement resolution, and there is complete left-right overlap.

The PLATE geometry is also distinguished from the PIPE geometry by the manner in which the photon x-angle is calculated. In the PIPE geometry, the emerging angles in both

planes are measured with respect to the bar axis.

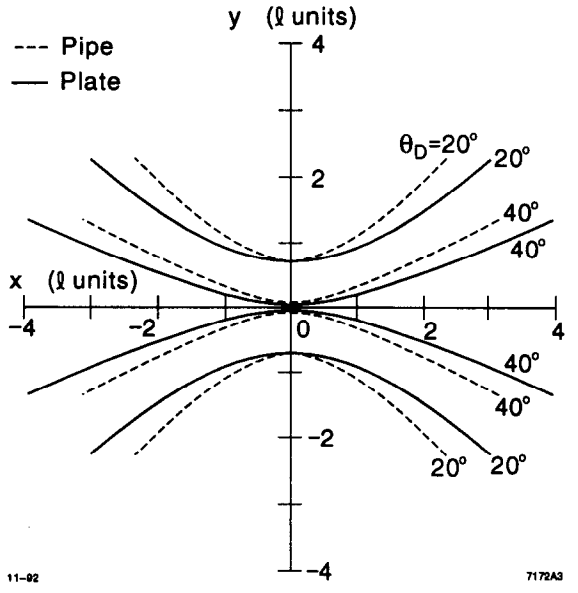

Figure 2. Loci of images for a $\beta = 1$ track at two different track dip angles produced by a single radiator of a DIRC counter on a plane surface placed at distance ℓ from the end of the radiator, in the zero thickness (t_y) limit. The track azimuthal angle (dx/dy) is zero. The refractive indices of the radiator and the detector standoff regions are $n_1 = 1.474$ and $n_2 = 1.0$, respectively. The dashed and solid lines correspond to different limits on the width (t_x) discussed in the text.

Thus, the bar dimensions must be substantially smaller than the photon detector resolution so as not to affect the angular measurement. In contrast, in the plate geometry, the angle in the x direction is measured with respect to the source track, and only the y-angle is measured with respect to the bar axis. The PLATE geometry has fewer ambiguities in the case where it is geometrically feasible to make the plate very wide (perhaps in a fixed target environment), but it does not seem possible to devise a full acceptance counter for a solenoidal detector at a collider without a significant number of photon bounces from the sides. Unless the PLATE has a large width/length ratio, the image depends in detail on the number of bounces, the width of the radiator, the position of the track in the radiator bar, etc., and consists of a number of disconnected pieces as shown in Fig. 3.

These individual pieces can themselves overlap and provide significant ambiguity, although some of the ambiguities may be removed using the timing dimension.

The PLATE geometry has the conceptual advantage that it removes the bar width t_x from the determination of the photon x-angle, provided, of course, that the number of bounces can be determined. This could be useful in some focusing geometries. It also has many fewer surfaces and would probably be cheaper to manufacture. However, it is simplest conceptually to image with respect to the PIPE and to accept the left/right imaging ambiguity implied, as we will do in the remainder of this paper. Then, in the limit of infinite transmission coefficient and small pipes, the observed image is dependent only on the track velocity and angles with respect to the bar, and independent of position in the bar [5].

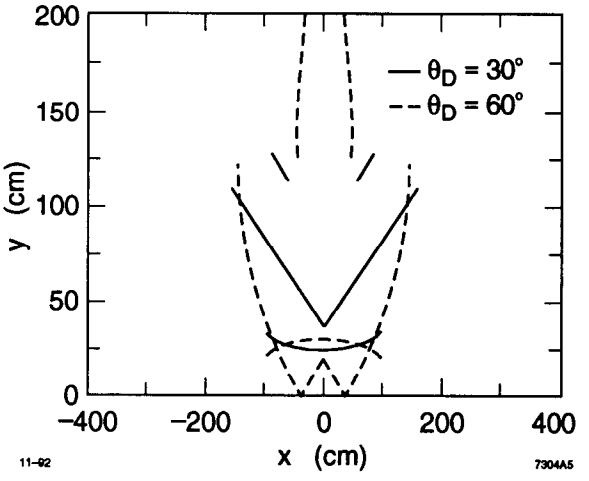

Figure 3. Loci of images for a $\beta = 1$ track for $\theta_D = 30^\circ$ (solid line) and $\theta_D = 60^\circ$ (dashed line) produced by a single PLATE radiator of a DIRC counter under conditions specified for Fig. 1. The plate width (t_x) is 100 cm and the track penetrates the plate 100 cm from the end with an azimuthal angle of zero.

Not all Cherenkov photons produced in the radiator can be collected by the detector. Some

photons are produced at angles below the total internal reflection limit and emerge from the faces of the radiator while others can be trapped in the radiator bar and lost. In order to cover the full acceptance aperture, it is necessary to fill the standoff region between the radiator end and the detector with a material whose index is substantially higher than 1.0. In particular, if the region at the radiator end is filled with a material with the same index as the radiator (i.e. $n_1 = n_2$), then the images will emerge without reflection or refraction at the end surface. Figure 4 shows the Cherenkov photon transport efficiency as a function of track β in this case, for a very simple model without absorption. The internal reflection coefficients are taken to be zero below the total internal reflection limit or one above. There are two distinct cases, corresponding to track dip angles lying either above or below the internal reflection limit of 47.3°. For the first case, the minimum transmission occurs at $\beta = 1$. It is maximum at Cherenkov threshold, and exceeds 60% for all particle velocities above the Cherenkov threshold. For the second case, the maximum transmission occurs at $\beta = 1$, and falls to zero below a cutoff β which lies above the Cherenkov threshold. In any case, the nominal transmission exceeds 45% for all angles when β exceeds 0.93, which corresponds to P_π = 0.35, and P_K = 1.24 GeV/c. Below 1.24 GeV/c, a DIRC with these parameters will function as a threshold Cherenkov for π/K separation over the central part of the angular acceptance, and will be unable to distinguish kaons from protons there.

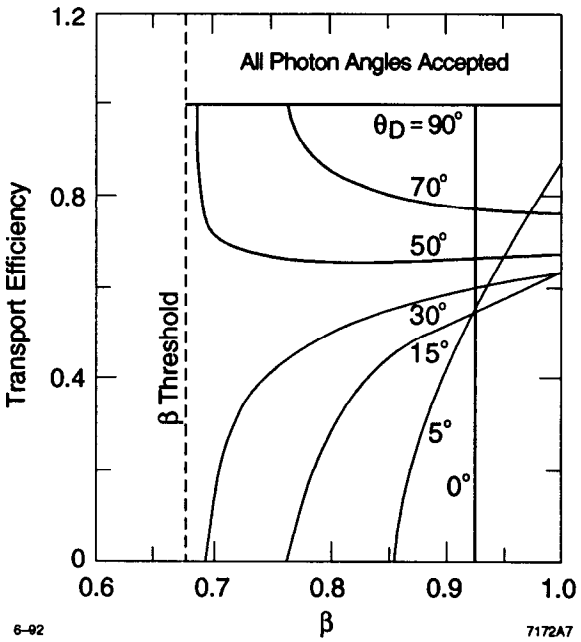

Figure 4. The fraction of Cherenkov photons transmitted to the detector as a function of β in the simple model described in the text. The refractive indices of the radiator and the detector standoff regions are equal.

3. THE RADIATOR

For a solenoidal geometry, each radiator bar must have very long Cherenkov photon absorption length and high quality surface finish (for good transmittance down the bar); flat, orthogonal surfaces (for accurate image transmission); low chromatic dispersion (to allow a good measurement of the Cherenkov angle); appropriate index of refraction (to transmit light down the bar); and preferably, long radiation length. Though a short device could be built using one of the fluoride glasses (e.g., LiF or CaF_2) operating in the TMAE regime, we know of no material suitable for operation of a long device (e.g., 2–6 m) in the 1700–2000 A° region where TMAE is sensitive. The "obvious" radiator choice for a long device is quartz, working in the visible to near UV range (i.e., 3000-6000 A°). As shown in Fig. 5, it has a transmission length which exceeds 50 m over most of this wavelength range; takes a high quality polish so that internal reflection coefficients can be made high; has the lowest dispersion of the oxide glasses (Abbe number 67.8); and can be procured in large pieces at relatively modest cost.

The standoff region (n_2) material between the detector and the radiator bar should be well matched in refractive index to the radiator and should have a rather long absorption length. It

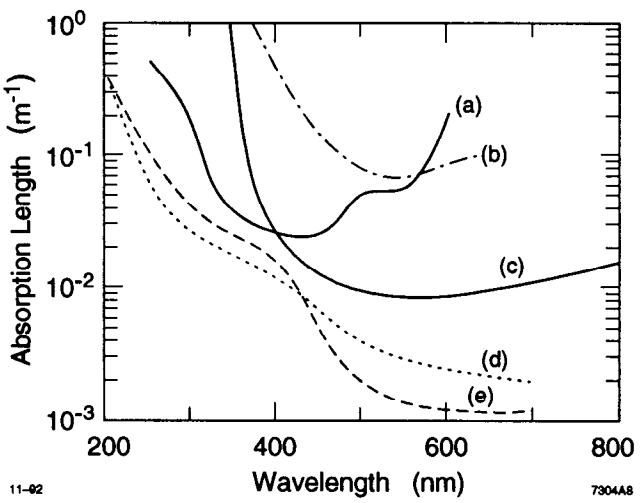

Figure 5. Examples of absorption lengths as a function of wavelength for some potential radiator and standoff region materials: (a) water (IMB quality) [6], (B) UVT acrylic [7], (c) laser liquid 3421 [8], (d) fused silica fiber [9], (e) bulk fused silica [10].

could be the same material as the radiator bar, but in the case of quartz bars, it seems more likely that the region would be filled with a liquid. Though there are liquid materials available which match the refractive index of quartz extremely well, their transmission in the near UV tends to be inadequate. Figure 5 shows the response of two candidate liquids which do have reasonable UV transmissions, curves (b) for water [n_2 =1.34], and (c) for Cargille Labs laser liquid 3421 [n_2 =1.41]. Water is inexpensive and quite transparent over the required range but would lead to some modest reflective losses at the n_1, n_2 interface for large angles. Liquid 3421 has a somewhat better refractive index match but cuts off earlier in 3000-4000 A^0 range, which would reduce the effective N_0.

For the rest of this paper, we will assume for simplicity that the radiator bars are made of quartz with index of refraction n_1 = 1.474, when weighted by the Cherenkov spectrum and the photodetector response, and will also assume that n_1 = n_2. Other alternatives are discussed elsewhere [3].

4. THE PHOTODETECTOR

The number of Cherenkov photons produced and transmitted to the detector surface is generally small, so it is important to obtain good efficiency from the photodetector. Moreover, since the position of each photon must be detected, the single photon signal-to-noise ratio must be very good. The photodetector surface must sit some minimum distance away from the radiator end (to obtain adequate resolution). Finally, the detector should be rather fast.

The "classic" device which fulfills these conditions is the photomultiplier tube, and a photodetection surface can be made of an array of these tubes. A photomultiplier is modestly efficient for single photoelectrons, has extremely good signal-to-noise, is fast, and can cover large areas at modest cost. The packing fraction in a closely packed array is typically 66%. For definiteness in the remainder of this paper, we will assume that the photodetector is made of a closely packed photomultiplier array arranged in a standoff geometry to provide a measurement of angle with respect to the bar. This has the conceptual "advantage" that the detector uses completely "conventional" technology whose performance is well understood and can be reliably simulated. Such a detector is self-triggering and fast. Not only does it allow reliable tagging of beam crossings (which are about 4 ns apart), but it should also be a good TOF counter. The timing resolution will also provide modest spatial resolution (~ 10 cm for a typical PMT) along the bar, and can be used to separate the direction of the photon if a reflective surface has been used on one end. Alternatively, the timing provides a measure of the photon path length to the photodetector. Since this depends on the light propagation angles, and production point in the bar, it provides an independent measure of a particular convolution of the Cherenkov angles, which could be

useful to improve the angle measurement in some cases, if the photon detector is very fast [11].

5. MODEL FOR B FACTORY DETECTOR

In this section, we will describe a particular model of a B factory detector which incorporates a DIRC. Many of the geometrical details of such a detector are arbitrary and many different models are possible. However, it is hoped that by discussing a specific choice, we can illuminate some of the trade-offs implicit in the design.

A view of the forward quadrant of this "model" B Factory detector is shown in Fig. 6. In order to bypass the difficult problem of keeping the end plate masses low in the central tracking devices, the particular geometry shown has no end caps. This also allows very uniform calorimetry and the simplest possible DIRC geometry. The "stretched" geometry is particularly attractive in this case because the inner radius of the calorimeter is small. The DIRC radiator consists of 1.23 x 4.0 x 560 cm (t_x, t_y, t_z) quartz bars. The radiator is 10% L_{RAD} thick radially and takes up to about 2.5 cm of radial space in all. The bars are placed on a 20 sided polygonal surface, as viewed from the end of the detector, and cover about 98% of the azimuth. The detectors are closely packed arrays of conventional photomultiplier (PMT) tubes at each end. As shown in Fig. 6, the surface is a cylindrical section in elevation and approximately toroidal as viewed from the end. The detector boxes have reflecting surfaces at the inner polygonal surface (approximately in the radiator x–z plane) and at $\tan^{-1}dy/dz = 1$ to save phototubes. They are filled with a fluid whose refractive index matches that of quartz, so there are no reflections at the radiator ends or phototube windows. The device works in the near ultraviolet and the visible. It is thin, compact, robust, very fast, and self triggering. The loci of Cherenkov images on a cylindrical detector surface for $\beta = 1$ tracks at a number of different dip angles are shown in Fig. 7 for the case where the track enters the radiator bar perpendicularly in azimuth ($\eta = 0$). The images are scaled for a standoff distance of 100 cm. Distortions in the image due to wrapping the detection cylinder around the beam pipe are neglected. The images at the detector for a particular dip angle ($\theta_D = 30^o$) are shown in Fig. 8 for three different angles in azimuth. For η angles other than zero, the images are "doubled" due to the side edge reflection ambiguity.

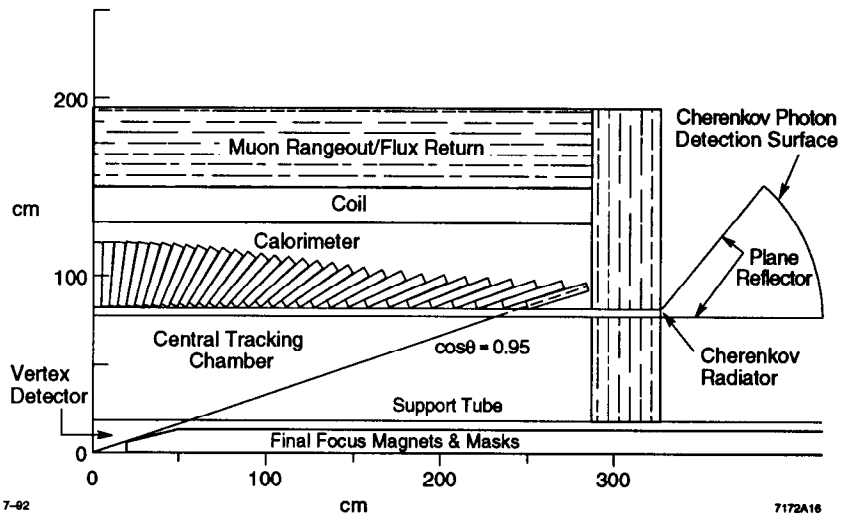

Figure 6. Schematic view of one quadrant of a model B factory detector incorporating a DIRC.

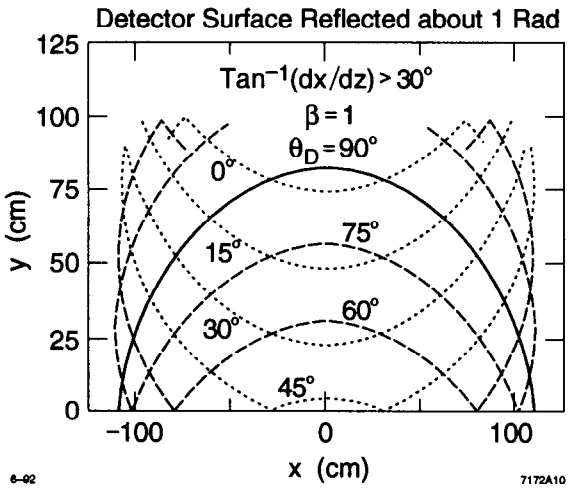

Figure 7. Loci of Cherenkov images from a $\beta = 1$ track on a cylindrical detection surface 100 cm from the radiator end. The track enters the radiator perpendicularly in azimuth. The detector surface is reflected at both 0 and 1 radians, and photons traveling down the bar with angles less than 30° are neglected.

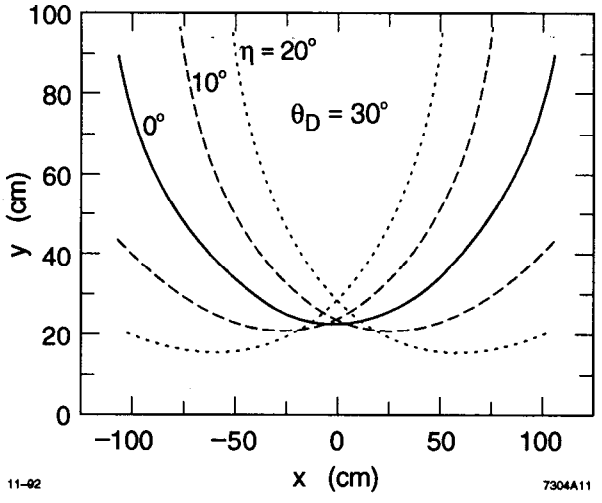

Figure 8. Loci of Cherenkov images from a $\beta = 1$ track on a cylindrical detection surface 100 cm from the radiator end. The track is at a dip angle (θ_D) of 30° and images are shown for three different azimuthal angles (η). The detector surface is reflected at both 0 and 1 radians, and photons traveling down the bar with angles less that 30° are neglected.

6. SIMPLE PERFORMANCE MODEL

In this section, we will discuss a simple model for the performance of a DIRC counter such as that described above to elucidate some of the important issues which determine performance. The number of photoelectrons (N_{PE}) produced in the photodetector can be written as:

$$N_{PE} = \frac{\varepsilon N_0 L \sin^2\theta_C}{\cos\theta_D} \quad . \quad (2)$$

where N_0 is the Cherenkov quality factor (about 100 cm^{-1} for a good bialkali phototube), L is the radial radiator thickness ($L = t_y = 1.23$ cm), and ε is the total collection efficiency. $\sin\theta_c$ for a $\beta = 1$ particle in quartz equals 0.735. ε has two main pieces. The first is the geometrical photon transport efficiency down the bar to the photodetector. This efficiency is a strong function of track dip angle and the azimuthal acceptance for photons in the bar. Second, closely packed PMTs only cover about 66% of the surface with an active photocathode, and it is difficult to increase the coverage much by collection optics due to the wide range of photon angles.

The number of photoelectrons N_{PE} expected for a $\beta = 1$ particle as a function of dip angle is shown in the following table:

Table 1: The number of photoelectrons expected for a β=1 particle as a function of dip angle.

θ_D	N_{PE}
0	27
15	17
30	22
50	56
70	83

The total separation in Cherenkov angle $\delta\theta_c$(tot) is given by

$$\delta\theta_c(\text{tot}) = \frac{\delta\theta_c}{\sqrt{N_{PE}}} \quad , \qquad (3)$$

where the angular error measurement from each photon detected $\delta\theta_c$ is

$$\delta\theta_c = \left(\begin{matrix}\delta\theta^2_{\text{Production}} + \delta\theta^2_{\text{Transport}} \\ + \delta\theta^2_{\text{Detection}}\end{matrix}\right)^{1/2} . \qquad (4)$$

6.1 $\delta\theta_{\text{Production}}$

The error associated with the Cherenkov photon production process $\delta\theta_{\text{Production}}$ is dominated by chromatic dispersion $\delta\theta_{\text{Chromatic}}$, and also includes contributions from multiple scattering $\delta\theta_{MS}$, and momentum bending in the radiator $\delta\theta_{\text{Momentum}}$. Dispersion in the radiator is the "fundamental" performance limit on attainable performance in an imaging Cherenkov. It is given by

$$\delta\theta_{\text{Chromatic}} = \frac{1}{\tan\theta_C}\frac{dn}{n} \quad . \qquad (5)$$

Thus, the chromatic dispersion contribution depends on the radiator dispersion averaged over the response of the photodetector. For a DIRC with a quartz radiator and bialkali photocathodes, this averaged value of dn/n is 5.8 mr, so that $\delta\theta_{\text{Chromatic}}$ is 5.4 mr for a $\beta = 1$ particle.

The errors associated with $\delta\theta_{MS}$ and $\delta\theta_{\text{Momentum}}$ are quite small and will be ignored.

6.2 $\delta\theta_{\text{Transport}}$

The smearing of the Cherenkov photons in transport $\delta\theta_{\text{Transport}}$ along the radiator bars is a function of a number of mechanisms. Some of these (e.g., small non-parallelism of the surfaces or a small number of well defined changes in bar angle) can be calibrated out, in principle. Others (such as surface "waves" or variations in refractive index) could lead to emittance growth and must be strictly controlled. Figure and surface quality specifications typical of optical components would be more than adequate. For example, a typical optical flat has a surface figure of about 1/8 λ, nearly three orders of magnitude better than these bars would require. Thus, the problem is not so much of principle, but rather economics. For the smearing calculation here, it will be assumed that quality can be sufficiently well controlled so that $\delta\theta_{\text{Transport}}$ can be ignored.

6.3 $\delta\theta_{\text{Detector}}$

The smearing of the photon angles due to measurement granularity comes from the size of the Cherenkov image (as formed by the bar dimensions) convoluted with the granularity of the photodetector surface, divided by the length from the radiator end to the detector. It is not "fundamental" but is driven by economics. For example, for a photon traveling in the y-z plane, if we assume a detector made up of closely packed 2 in. PMTs (with spatial resolution δy_{PMT}) located at 165 cm (L) from the end of the 1.23 cm thick radiator.

$$\delta\theta_{\text{Detector}} \approx \sqrt{\left(\frac{\delta y^2_{PMT} + \delta y^2_{\text{radiator}}}{L^2}\right)} = 6.8\text{mr} \cdot \qquad (6)$$

An array of 1 in. tubes at 95 cm give the same resolution.

6.4 Performance

The performance of any imaging Cherenkov is a strong function of momentum, of course, because the angular separation between particle species is such a rapidly varying function of momentum. The expected π/K separation versus momentum is shown in Fig. 9. There is

a natural enhancement of the separation at the forward angles due primarily to the increasing number of photons detected. Since the asymmetric machines can only produce the fastest particles at large dip angles, the detector described above actually has over 5σ separation for all B factory tracks. Even a device with $\delta\theta_{Detector}$ = 10 mr would have over 4σ separation for all B factory tracks.

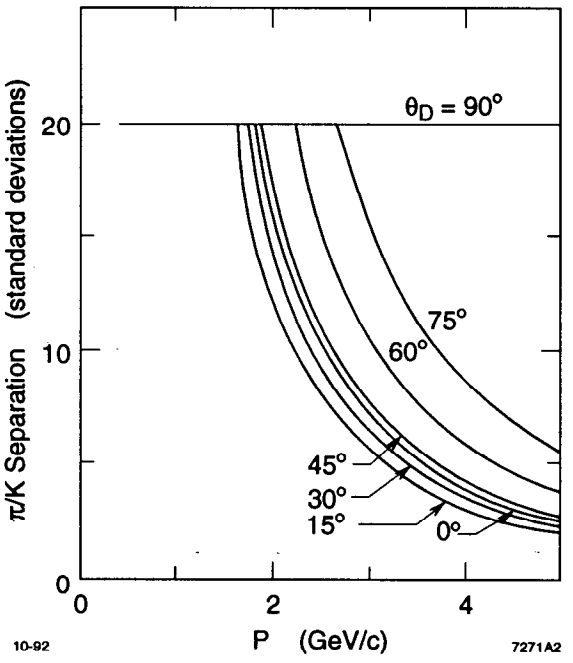

Figure 9. The predicted π/K separation as a function of momentum in a DIRC counter with a detector resolution of 6.8 mr. The lines show the dependence for a variety of track dip angles θ_D.

7. COMMENTS ON THE DETECTOR MODEL

A few comments follow on choices made in the model detector and some possible changes to the model. Most of these issues are discussed in more detail elsewhere [3].

7.1 Penetration of the Magnet Pole Pieces

The solution discussed above requires essentially complete azimuthal penetration of the pole pieces by the light bars. This requires an external support structure for the end "plug" of the magnet pole piece, with the photodetection surface probably lying inside the support structure. Though this is clearly an unusual requirement on the pole piece structure and requires a detailed engineering analysis, it does seem feasible.

There are many other options for penetrating the magnet pole pieces which can be considered, but all have some potential difficulties, typically lead to some compromise in performance, and require understanding the magnet design in more detail. The best solution of all would be to find photodetectors with adequate performance that would operate in a magnetic field (see section 7.3).

7.2 Endcaps

The endcap-less detector configuration described above is very uniform and avoids the problems created by particles penetrating the central tracking endplates, but it does lead to long detectors. It is possible to build a DIRC with an endcap if it were required. However, it might need to be somewhat thicker than the barrel device for equal performance, and readout of the combined bars would be significantly more difficult.

7.3 Detector Issues

The number of PMTs required for a DIRC is large and a major component of the cost. Essentially, the detector resolution specification "fixes" the number of pixels required to cover a certain solid angle, as viewed from a single radiator bar. Of course, in the model device, the same pixels are view many radiator bars. Pixels must be placed sufficiently far away from the radiator end to reach the required resolution. Thus, in the limit that the bar size is negligible, the number of pixels required for a single bar device is an invariant. For a finite sized bar, the size required for these pixels is dependent on the nature of the focusing system. For the non-focusing standoff system discussed

above, there is a simple relationship between pixel size and the distance between the radiator end and the detector surface (see Sec. 6.3). Minimization of the detector cost, while keeping the track overlap problem under control, tends to lead to tubes in the 2 in. range, but most other considerations would argue for smaller tube sizes. If very fast photodetectors could be used, the measurement of angle from the time dimension may become competitive with that available from position. This might allow a design with lesser resolution in one or both of the position measurements. Alternatively, in a high background environment, excellent time resolution will lead to better background rejection.

Mesh phototubes provide substantial immunity to magnetic fields. However, presently available tubes do not have very good performance in the single photoelectron regime. Their cathode sensitivity is generally about 60% that of a good conventional tube, and they do not have a good single photoelectron peak. As an estimate, they might be expected to provide about 50% of the photoelectrons observed by a good conventional tube.

In principle, a focusing system can be devised which will compensate for the finite size of the detector bar. This might allow the use of a rather small detection surface, with a very small pixel size, if an appropriate detector can be found. Possible candidate detectors are micro channel plate (MCP) PMTs; multianode PMTs [12]; and silicon photodetectors[13, 14]. Significant progress has been made in many of these devices in the last few years. However, at the moment we are not aware of any commercially available devices that meet all the necessary criteria.

Finally, there are other mechanisms for obtaining information on the photon angle other than the standoff and focusing schemes discussed here [15]. Some of these schemes are conceptually attractive and should be considered carefully.

7.4 Costs

The cost optimization of a DIRC is a complex multiparameter problem, and depends on many of the design choices. In general, radiator thickness can be traded for tube performance or radiator quality, and the number of channels can be traded against per-channel cost and desired performance. Although radiator manufacturing issues are probably the least well understood technically, the cost will almost certainly be dominated by per-channel detection and readout costs. As a very rough guess, the model device discussed above would cost about 10 M$. Space inside a crystal calorimeter is extremely expensive. For example, if a DIRC saves 15 cm of space which allows a smaller calorimeter, the cost savings from CsI volume alone would be in the 6–10 M$ range. In this sense the DIRC might be said to "pay for itself."

8. Conclusion

The DIRC has many attractive features and appears to be extremely well matched to the requirements for a particle identification device at the B factory. Of course, there are a number of potential problems that need to be addressed for the DIRC, and since it is a new device, a full scientific prototype is highly desirable. The number of photodetection pixels required is quite large (of order 10,000 or more), so the cost will probably be rather large. There is a "conventional" commercially available choice available for the photodetection surface (PMTs), although other techniques might be preferable if they become available. The most uncertain elements to manufacture are the radiator pieces. Though the finish specifications are not particularly severe by high–end optical industry standards, the pieces are very large and it will be a major challenge to produce them in the sizes required and still keep costs under control. R&D is now centered on radiator production

and evaluation, photodetector evaluation and construction, and software studies, leading to the construction and testing of a physics prototype.

REFERENCES:

[1] SLAC-REP-373 (1991).

[2] For reviews, see e.g., B. Ratcliff, SLAC-PUB-5853 (1992), and P. Coyle et. al., SLAC-PUB-5594 (1991).

[3] B. Ratcliff, BaBar Note 92 (1992), and SLAC-PUB-5946 (1992).

[4] P. Baillon, NIM A238 (1985) 341; S. Yellin, CRID analysis internal note.

[5] For a simple analytic treatment of image formation, see, Blair Ratcliff, Presentation to the PEP-II Particle Identification working group, July 1992.

[6] R. M. Bionta et al., Proceedings of the 17th Rencontre de Moriond (1982).

[7] G. Kettenring, NIM 131 (1975) 451; manufacturers data, Rohm and Haas, Philadelphia, PA.

[8] R. P. Cargille Labs, Cedar Grove, NJ, USA.

[9] Fiberguide Industries, Stirling, NJ, USA.

[10] Melles Griot, Irving, CA, USA.

[11] The use of time-correlated information has been emphasized by M. Selen and K. Honschied in their proposal for reading out a DIRC bar using only the time dimension (private communication, CBX92-116).

[12] For a discussion of tests of some of these devices see, e.g., C. Jeanney, DPhePE 91-07 (1991).

[13] See for example, Advanced Photonics, Camarillo, CA.

[14] M. Atac et al., Nucl. Instrum. Meth. A320 p. 1255-160 (1992).

[15] See for example, B Ratcliff in BaBar Note 37, and P. Coyle, Presentation to the PEP-II Particle Identification Working group, April 1990.